Magnetic Resonance in Medicine 47:967–972 (2002)
DOI 10.1002/mrm.10144

White Matter Mapping Using Diffusion Tensor MRI

C.R. Tench,[1*] P.S. Morgan,[2] M. Wilson,[1] and L.D. Blumhardt[1]

Diffusion tensor MRI is used to define trajectories that reflect the long-range order of in vivo white matter (WM) fiber tracts. Fiber tracking is particularly prone to cumulative error from noise and partial volume along the length of the trajectory paths, but the overall shape of each path is anatomically meaningful. By considering only the long-range similarity of path shapes, a method of constructing 3D maps of specific WM structures has been developed. A trajectory is first computed from an operator-selected seed voxel, located within the anatomical structure of interest (SOI). Voxels from the same structure are then automatically identified based on the similarity of trajectory path shapes, assessed using Pearson's correlation coefficient. The corpus callosum and pyramidal tracts in 14 patients with multiple sclerosis, and in 10 healthy controls were mapped by this method, and the apparent diffusion coefficient (ADC) was measured. The ADC was significantly higher in patients than in controls, and higher in the corpus callosum than in the pyramidal tracts for both groups. Using this method the different functional structures in the WM may be identified and mapped. Within these maps, MRI parameters can be measured for subsequent comparison with relevant clinical data. Magn Reson Med 47:967–972, 2002. © 2002 Wiley-Liss, Inc.

Key words: diffusion tensor; tractography; multiple sclerosis; corpus callosum; pyramidal tracts

The diffusion tensor imaging (DTI) modality is a recent development in MRI. Data acquired by DTI is used to construct a diffusion tensor in each voxel (1–3). The tensor describes the quantitative apparent diffusion properties local to that voxel through its eigenvalues and eigenvectors. This is fundamentally different from other modalities wherein each voxel contains only a scalar signal intensity.

Diagonalizing the diffusion tensor yields three eigenvalues, each of which measures the apparent diffusion coefficient (ADC) in one of three orthogonal directions. In the brain, the random motion of the water molecules in cerebrospinal fluid (CSF) and gray matter (GM) ensures largely isotropic diffusion. In the white matter (WM), restricted movement of water perpendicular to the direction of the fiber tracts results in anisotropic diffusion, so that one eigenvalue is significantly larger than the others. The largest eigenvalue is associated with the major diffusion vector, which has been shown to point parallel to the fiber tracts (4) and provides a means of mapping specific tract bundles (5–8). The method described here utilizes the major diffusion vector to define trajectory paths that reflect the underlying shape of these bundles.

Analysis of specific WM structures is important because the functional role of each is different. The ability to identify and segment a single structure would allow a detailed assessment of damage within it, and a subsequent comparison with relevant clinical data (9). With conventional MRI, a brain atlas may be used to map the different regions (10). This is, however, subject to error due to intersubject anatomical variability (8,9). Since the advent of DTI, several groups have attempted to utilize the vectorial information available from the diffusion tensor to identify different structures. Specific WM tract bundles have been identified by computing trajectories initialized from within regions of interest (ROI) (5,11). This method was used by Basser et al. (5) to map the pyramidal pathways and the corpus callosum, and produced anatomically plausible results. The problem indicated by the study was the ability of trajectories to jump to adjacent structures via noisy or partially volumed voxels. Further, the final result was sensitive to the placement of the ROI; trajectories emanating from the ROI might therefore execute a different path for a small displacement in start position, reducing the repeatability of such methods. Jones et al. (6) used a different approach based on a compatibility measure that considered both the vectorial data and the anisotropy of the diffusion coefficients. The method compared the 26 nearest-neighbor voxels in order to cluster those with high compatibility. This resulted in groups of voxels within a single structure having the same classification. However, the classification was incomplete and resulted in fragmentation of the structures.

In this work we describe a method of producing a 3D map of a specific WM structure of interest (SOI). It relies on the long-range similarity of WM fibers from the same tract bundle, and the anatomical plausibility of trajectories as defined by DTI (5). From an initial seed point, a 3D connected region is grown to include only voxels from the same anatomical SOI. The trajectory originating from each potentially connected voxel must correlate sufficiently strongly with the seed trajectory for a connection to be made. Therefore, only the trajectory shapes are important in our technique, rather than the details of the paths, which may not be so reliable. We use the method to map the corpus callosum and the pyramidal tracts in 14 patients with multiple sclerosis (MS), and in 10 control subjects. We then compare the apparent diffusivity within these structures.

METHOD

The macroscopic shape of functionally specific WM structures reflects the long-range order of the constituent fiber tracts. In simple structures each tract is highly similar in shape, differing only by a trivial spatial translation. In more complex structures, such as the corpus callosum, there is a slow variation in the shape of the fiber tracts in

[1]Division of Clinical Neurology, University Hospital, Nottingham, UK.
[2]Division of Academic Radiology, University Hospital, Nottingham, UK.
*Correspondence to: C. Tench, Division of Clinical Neurology, University Hospital, Derby Road, Nottingham NG7 2UH, UK. E-mail: msxct@nottingham.ac.uk
Received 9 November 2001; revised 9 January 2002; accepted 24 January 2002.

addition to a translation. Trajectories defined using DTI have been shown to reflect the local shape of the tract fibers (5). The task of identifying a specific SOI in WM is therefore reduced to identifying connected voxels in the diffusion tensor data that yield similar trajectories. Here we have used Pearson's correlation coefficient (12) to define the similarity between trajectories.

Clinical Data Acquisition

We applied our method to 14 patients with MS, and 10 healthy controls. Approval was obtained from the local ethics committee, and all subjects gave informed consent.

MRI

All subjects were scanned in a clinical imaging system at 1.5T (Magnetom Vision; Siemens, Erlangen, Germany). We used a spin-echo, echo-planar, diffusion-weighted sequence (128 × 128 matrix, TE = 103 ms, TR = 6000 ms, time per echo = 0.8 ms, number of echoes = 96, voxel dimensions 2 × 2 × 4 mm). Diffusion weighting was achieved by the application of Stejskal-Tanner diffusion gradients (13) with $b_{\max} = 1000$ s/mm^2. Seven images are necessary to construct the tensor: six in the presence of noncolinear diffusion gradients, and one with no gradient field (2). A total of 15 axial slices were imaged, sampling a volume that encompassed the lateral ventricles and included the cerebral peduncles and midbrain in the most caudal slices.

Postprocessing of MRI Data

Echo-planar imaging is highly susceptible to magnetic field inhomgeneities, leading to significant spatial distortion of the acquired data. We make a correction for this distortion (14) before using the data to construct the tensor.

The necessity for reasonable acquisition times in a clinical environment dictates the resolution and signal-to-noise ratio (SNR) of MRI data. With the current imaging technology, DTI suffers from a significant degree of noise for any useful voxel size. Parameters derived from the diffusion tensor, including the major diffusion vector, may be highly sensitive to such noise. In an attempt to counter this we apply Gaussian filtering to the MRI data, which results in more robust tensor-derived parameters (15–17) and better contrast between the WM, CSF, and GM.

Tensor Digitalization

The processed MRI data is used to construct a 3 × 3 symmetric diffusion tensor **D** in each voxel. The three apparent diffusion coefficients (ADCs) λ_i are obtained from the tensor by solving the characteristic equation (18) $(\mathbf{D} - \lambda_i\mathbf{I}) = 0$, where **I** is the identity matrix. The three orthogonal diffusion directions then follow from the cofactors of the matrix (18) $(\mathbf{D} - \lambda_i\mathbf{I})$.

Images

Three image types derived from the tensor are used. The first is a scalar map of relative anisotropy (RA), as defined in Ref. 2, which measures the relative differences between the three ADCs. These images are of high intensity in WM but low intensity in GM and CSF, as shown in Fig. 1a. The ADC image, Fig. 1b, is also a scalar map, where each voxel contains the mean of the diagonal elements of **D**. This reflects the direction-averaged apparent diffusivity within the voxel. In the third image type, each voxel contains the normalized major diffusion vector. To visualize the vectorial information, a different color is used to denote each direction and the vector is scaled so that its magnitude is equal to the RA (an example is shown in Fig. 1c). Here we use blue to represent the *x* component, green to represent the *y* component, and red for the *z* component. The length of each vector component is represented by the intensity of the relevant color.

Image Processing

Since we are interested only in the WM, the GM and CSF are removed using a semiautomated seeded region growing method on the RA images. The resulting WM map defines the limits for our tractography procedure.

WM Tractography

The procedure for mapping tracts from an initial point $\mathbf{r}_0$ to a final point $\mathbf{r}_N$, through all intermediate points $\mathbf{r}_n$, is summarized by the equation

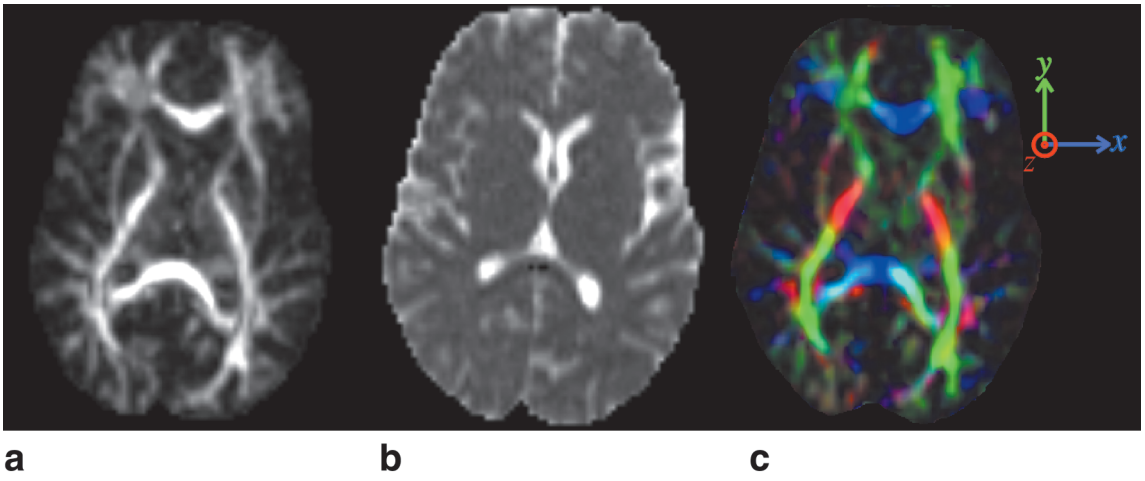

FIG. 1. **a:** RA image. **b:** ADC image. **c:** Major diffusion vector, scaled by RA.

$$\mathbf{r}_{n+1} = \mathbf{r}_n + h\mathbf{V}_{n+1} \quad [1]$$

and shown graphically in Fig. 2. Here h is a step length parameter and $\mathbf{V}_n$ is derived from the major diffusion vector using a fourth-order Runga-Kutta method (19). The trajectory can only be defined once the initial conditions $\mathbf{r}_0$ and $\mathbf{V}_0$ have been specified.

The step length h is established such that convergent results are obtained, i.e., halving the step size has no effect on the trajectory path; here we use $h = 1$ mm, which is half the smallest linear dimension of a voxel. To obtain $\mathbf{V}_n$, the MRI data is interpolated in three dimensions using a linear Lagrange interpolating polynomial (19). The major diffusion vector may then be calculated as a continuous, normalized vector field $\mathbf{E}(\mathbf{r})$. Then, for $n \geq 0$,

$$\mathbf{V}_{n+1} = \frac{1}{6}(\mathbf{k}_1 + 2\mathbf{k}_2 + 2\mathbf{k}_3 + \mathbf{k}_4), \quad [2]$$

where

$$\mathbf{k}_1 = \frac{\mathbf{V}_n \cdot \mathbf{E}(\mathbf{r}_n)}{|\mathbf{V}_n \cdot \mathbf{E}(\mathbf{r}_n)|}\mathbf{E}(\mathbf{r}_n), \quad [3]$$

$$\mathbf{k}_2 = \frac{\mathbf{V}_n \cdot \mathbf{E}(\mathbf{r}_n + h/2\mathbf{k}_1)}{|\mathbf{V}_n \cdot \mathbf{E}(\mathbf{r}_n + h/2\mathbf{k}_1)|}\mathbf{E}(\mathbf{r}_n + h/2\mathbf{k}_1), \quad [4]$$

$$\mathbf{k}_3 = \frac{\mathbf{V}_n \cdot \mathbf{E}(\mathbf{r}_n + h/2\mathbf{k}_2)}{|\mathbf{V}_n \cdot \mathbf{E}(\mathbf{r}_n + h/2\mathbf{k}_2)|}\mathbf{E}(\mathbf{r}_n + h/2\mathbf{k}_2) \quad [5]$$

and

$$\mathbf{k}_4 = \frac{\mathbf{V}_n \cdot \mathbf{E}(\mathbf{r}_n + h\mathbf{k}_3)}{|\mathbf{V}_n \cdot \mathbf{E}(\mathbf{r}_n + h\mathbf{k}_3)|}\mathbf{E}(\mathbf{r}_n + h\mathbf{k}_3). \quad [6]$$

Defining $\mathbf{V}_n$ in this way ensures that $\mathbf{V}_n \cdot \mathbf{V}_{n-1} \geq 0$, i.e., the angle subtended between successive vectors is $\leq 90°$. This is necessary since the sign of $\mathbf{E}(\mathbf{r})$ is arbitrary. This stepwise mapping procedure defines a trajectory, as depicted in Fig. 2, which continues to a point $\mathbf{r}_N$. The trajectory is terminated when a predefined stopping criteria is met.

A complete trajectory path $\mathbf{R}$ is defined in two parts. First,

$$\mathbf{R}_n = \mathbf{r}_n[0 \leq n \leq N] \text{ with } \mathbf{V}_0 = \mathbf{E}(\mathbf{r}_0)$$

describes a trajectory moving away from $\mathbf{r}_0$ in an initial direction $\mathbf{E}(\mathbf{r}_0)$. Second,

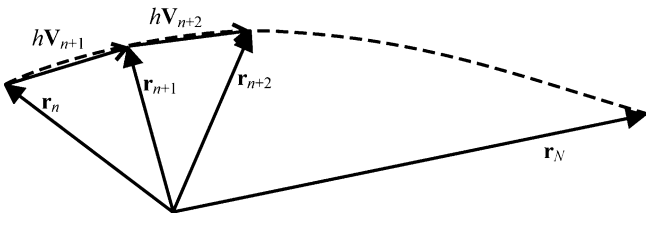

FIG. 2. The principle of tractography.

$$\mathbf{R}_{-n} = \mathbf{r}_n[0 \leq n \leq N'] \text{ with } \mathbf{V}_0 = -\mathbf{E}(\mathbf{r}_0)$$

describes a trajectory moving away from $\mathbf{r}_0$ in an initial direction $-\mathbf{E}(\mathbf{r}_0)$. The complete trajectory is described by $\mathbf{R}_i$ $[-N' \leq i \leq N]$, where N' and N are the termination points. For the purposes of correct comparison of trajectories, it is necessary to occasionally reverse this definition such that $\mathbf{R}_n = \mathbf{r}_n$ $[0 \leq n \leq N]$ with $\mathbf{V}_0 = -\mathbf{E}(\mathbf{r}_0)$ and $\mathbf{R}_{-n} = \mathbf{r}_n$ $[0 \leq n \leq N']$ with $\mathbf{V}_0 = \mathbf{E}(\mathbf{r}_0)$.

Stopping Criteria

Left to itself, a trajectory would continue until its path reached the edge of the data defined by our WM map. Unfortunately, the reliability of the tracking is compromised by the noise and degree of partial volume in the image, meaning that trajectories tend to jump between adjacent WM structures. This usually happens when a trajectory undergoes a sharp change in direction. We apply a maximum allowable rate of change of direction, accepting only gentle curvature along the trajectory, in an attempt to constrain the path to one structure only. We find that a maximum of 10° per 1-mm step allows anatomically reasonable curvature while stopping trajectories that undergo unexpected directional changes. We further apply a lower RA threshold of 0.05; a trajectory passing through a voxel with RA lower than this is immediately terminated. This low RA threshold serves only to terminate the procedure at the edge of the WM data. A higher threshold is undesirable because it could potentially stop trajectory paths from traversing regions of abnormally low RA, such as MS lesions (20).

Correlations Between Trajectories Originating From Different Voxels

The method used in this study requires the measure of similarity between different 3D trajectories. Two trajectory paths, $\mathbf{R}^i{}_n$ $[-N'^i \leq n \leq N^i]$ and $\mathbf{R}^j{}_n$ $[-N'^j \leq n \leq N^j]$, originating from voxels i and j, respectively, may be compared using the vector form of Pearson's correlation function,

$$\mathbf{r}_{ij} = \frac{\sum_{n=-a}^{b} (\mathbf{R}^i_{n+p} - \overline{\mathbf{R}^i_{n+p}}) \cdot (\mathbf{R}^j_{n+q} - \overline{\mathbf{R}^j_{n+q}})}{\sqrt{\left[\sum_{n=-a}^{b} |\mathbf{R}^i_{n+p} - \overline{\mathbf{R}^i_{n+p}}|^2\right]\left[\sum_{n=-a}^{b} |\mathbf{R}^j_{n+q} - \overline{\mathbf{R}^j_{n+q}}|^2\right]}}. \quad [7]$$

In this equation the integers p and q are chosen to minimize the distance $|\mathbf{R}^i_p - \mathbf{R}^j_q|$, defining an origin for the two trajectories that ensures they are compared "in phase." The summation limits are defined by $a = \min(N'^i + p, N'^j + q)$ and $b = \min(N^i - p, N^j - q)$. The vectorial means $\overline{\mathbf{R}^i_{n+p}}$ and $\overline{\mathbf{R}^j_{n+q}}$, are given by

$$\overline{\mathbf{R}^i_{n+p}} = \sum_{n=-a}^{b} \mathbf{R}^i_{n+p} \quad [8]$$

and

$$\overline{\mathbf{R}^j_{n+q}} = \sum_{n=-a}^{b} \mathbf{R}^j_{n+q}. \quad [9]$$

The correlation coefficient r_{ij} is normalized so that $-1 \leq r_{ij} \leq 1$, where 1 means an exact similarity. Negative values of r_{ij} may mean that one trajectory is reversed relative to the other. In this case, the trajectory $\mathbf{R}^j_n$ is reversed as described above to yield a positive correlation coefficient.

Algorithm

Here we describe the algorithm used to obtain a 3D connected object representing a specific WM SOI. The object consists of member voxels that are connected to a seed point that has been positively identified as part of the SOI by the operator. The seed point, say voxel *i*, becomes the first member of the object. Then for voxel *j*, which is not already a member of the object but has at least one neighboring voxel that is, the correlation coefficient r_{ij} is calculated. If r_{ij} is greater than some predefined threshold, then voxel *j* will become a new member of the object. This process is continued, effectively growing the seed, until no new members can be created. The algorithm was implemented in the C programming language using a recursive function (21).

The procedure is performed interactively. A seed is first picked by the operator from the color major diffusion vector image (Fig. 3). Then a region is grown from this point based on some minimum correlation coefficient. The minimum correlation is chosen to be as low as possible without including voxels that are not part of the SOI. Once an object is defined in this way it is stored. If a single seed point is insufficient to identify all voxels within the structure, then a new seed point is picked and a new region grown. When the operator is again satisfied that the object grown from this seed represents some part of the SOI, it is added to the original and stored. The process is complete when no new seed points can be identified.

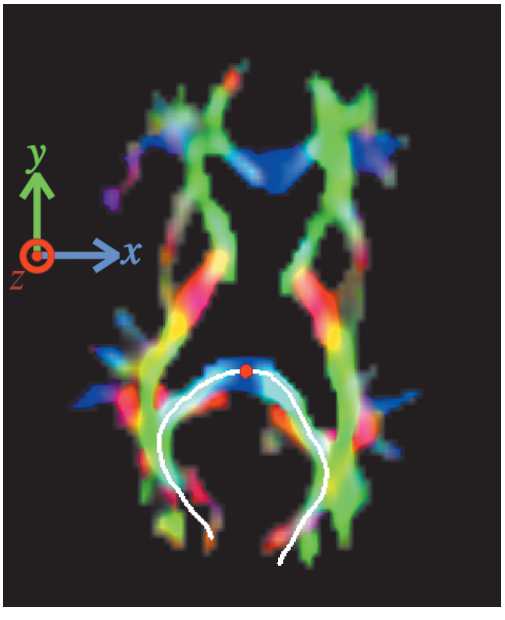

FIG. 3. Color major diffusion vector map of the WM only. The red circle indicates the seed point, and the white line a 2D projection of the trajectory.

Seed Point Selection

Selection of the seed point is the most critical aspect of the procedure. The trajectory originating from the seed must represent the shape of the SOI. Figure 3 shows a seed point located at the center of the splenium of the corpus callosum. The resulting trajectory, shown as a 2D projection, follows the expected path, not jumping to any adjacent structures via noisy or partially volumed voxels. This seed is primarily picked because of the shape of the resulting trajectory, but also because it is of high anisotropy, indicating deep WM. An object grown from this seed will certainly be part of the corpus callosum because of its unique shape compared to other WM structures.

To map the pyramidal tracts, seed points from the easily identified posterior limb of the internal capsule were selected. For the more complicated corpus callosum, seed points were selected from the genu, body, and splenium.

Experimental Procedure

Using the method described above, we obtained maps of the corpus callosum and pyramidal tracts for each subject. Figure 4 depicts the maps obtained in one control subject. We then calculated the median ADC value for each map, using all voxels identified. The Mann-Whitney *U*-test was used to test for differences between patients and controls, and for regional ADC differences. By repeating the procedure for five patients and five controls, we assessed the reproducibility of these measurements.

RESULTS

The ADC values obtained are summarized in Table 1. We found that the median ADC was higher in the patients than in the controls for both the corpus callosum ($P = 0.0018$) and the pyramidal tracts ($P = 0.0123$). Also, for both controls and patients the median ADC was significantly higher in the corpus callosum than in the pyramidal tracts ($P < 0.0001$). The coefficient of variation on repeating the mapping was 0.6% in the corpus callosum and 0.3% in the pyramidal tracts.

DISCUSSION

The introduction of DTI has made possible the visual identification of specific WM structures (22); this is a direct result of the vectorial information available. Yet only a fraction of the constituent voxels can be located in this way with certainty. The development of tractography promises more rigorous methods of identifying these structures by trajectory mapping of the WM fibers.

However, significant problems remain in the acquisition of diffusion tensor data. The low SNR of diffusion-weighted images forces the use of suboptimal image resolution. Tensor-derived parameters, such as RA and the major diffusion vector, are sensitive to these limitations (15). Tractography is particularly prone to noise due to cumulative error along the length of the trajectory path. This renders the end point of a

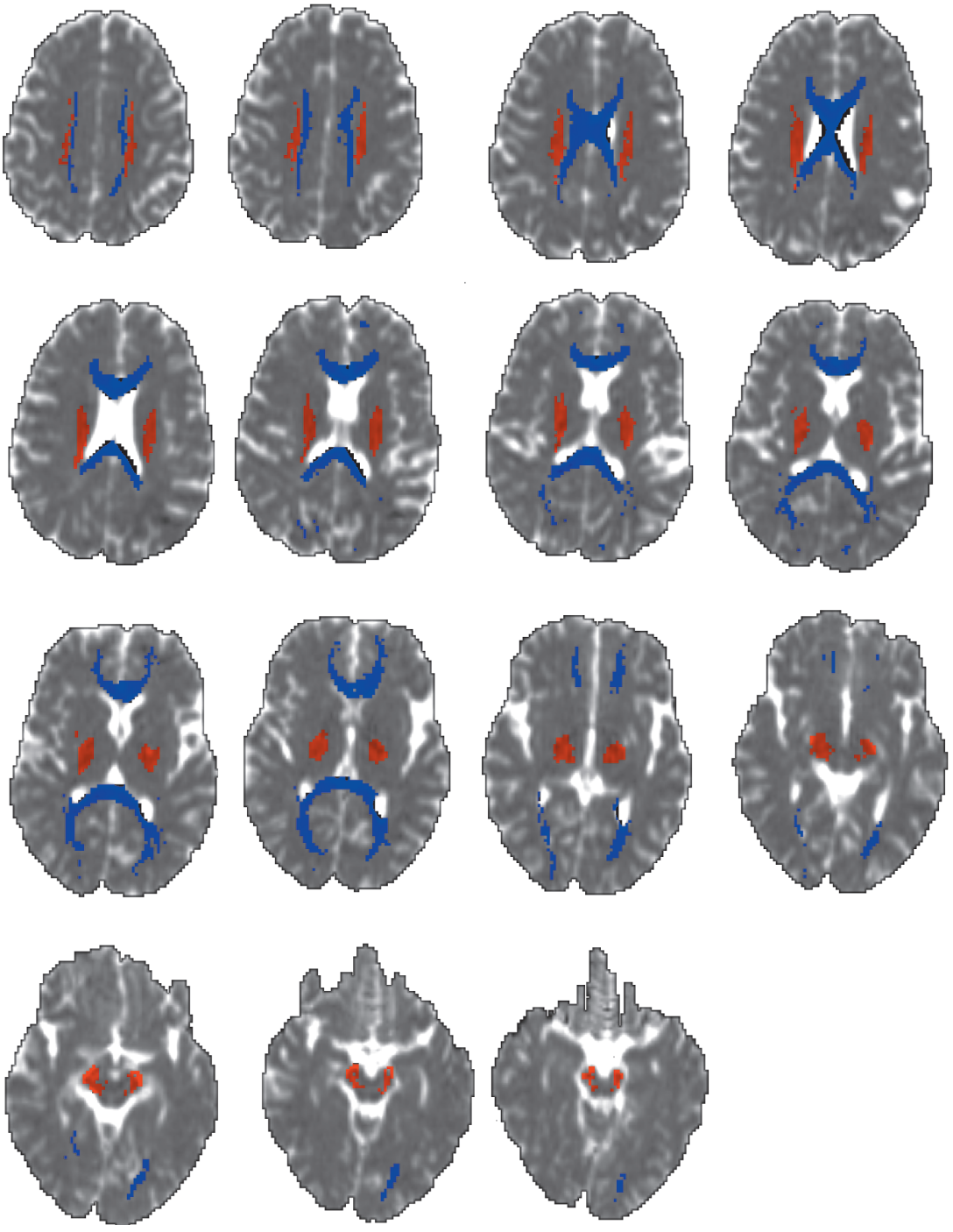

FIG. 4. Fifteen axial slices of the ADC image. Red pixels indicate the pyramidal tracts. Blue pixels indicate the corpus callosum.

trajectory highly sensitive to its start point. These problems need to be addressed before individual trajectories can be used to confidently infer WM connectivity between two distant points in the brain. Still, the overall shape of the trajectories has been shown to be anatomically meaningful, providing quantitatively useful data (5).

Image processing methods have been suggested to improve the robustness of the vectorial data. Gaussian smoothing was used by Westin et al. (17), and by us, to obtain a more stable estimate of the major diffusion direction. However, this reduces the effective image resolution, further increasing the problems with partial volume. A least-squares B-spline interpolation scheme has also been suggested (5) to improve the tracking process, but again this effectively reduces resolution. More sophisticated methods such as nonlinear smoothing (16) and statistical regularization of the directional data (8,23) may prove to be more useful in reducing random errors.

Further problems arise when applying DTI to a WM disease. Abnormalities such as MS lesions lead to regions of low anisotropy (20), where tractography is less reliable. This results from incorrect selection of the major eigenvector, when all eigenvalues are similar in magnitude (15,24), causing disruption of the trajectory path. The operator

Table 1
The ADC Values for Patients and Controls

	Corpus callosum		Pyramidal tract	
	ADC	SD	ADC	SD
Controls	0.77	0.027	0.71	0.016
Patients	0.82	0.044	0.74	0.022

Median ADC values (units $10^{-3}mm^2s^{-1}$).

method proposed by Westin et al. (17) may provide a solution to this problem.

The method described here provides a means of locating the voxels relevant to a single WM SOI. It relies on an operator-selected seed trajectory that conforms to the expected shape of the relevant structure. Voxels are then identified based on the statistical similarity of trajectories. With this approach it is the global shape of a trajectory that is important, rather than the fine details of its path. While the method still suffers from the general problems of tractography, relying only on the overall shape of trajectories gives it an inherent degree of noise and partial volume immunity. With the use of advanced tracking and image processing methods, as described above, our technique could be further improved.

We used the method to measure the ADC in the pyramidal tracts and the corpus callosum of both normal controls and patients with MS. The ADC was significantly higher in the patients than in the controls, in agreement with other studies (20,25–29). We also found that the ADC was higher in the corpus callosum than in the pyramidal tracts for both the control and the patient groups. This regional difference was not observed in a previous ROI study by Pierpaoli et al. (3). The coefficient of variation was less than 1% on repeating the procedure, indicating a high level of reproducibility.

CONCLUSIONS

We have developed a method to produce anatomically plausible maps of specific WM structures using the DTI modality. The method was used to map the corpus callosum and pyramidal tract structures in patients with MS, and in normal controls. Analyzing these structures revealed a significantly increased ADC in the patients. We also observed significantly higher ADC in the corpus callosum than in the pyramidal tracts for both groups. Good reproducibility of the method is indicated by the low coefficient of variation on repeating the mapping. This may be due to the inherent noise immunity of the mapping procedure.

REFERENCES

1. Le Bihan D, Mangin JF, Poupon C, Clark CA, Pappata S, Molko N, Chabriat H. Diffusion tensor imaging: concepts and applications. J Magn Reson Imaging 2001;13:534–546.
2. Basser PJ, Pierpaoli C. A simplified method to measure the diffusion tensor from seven MR images. Magn Reson Med 1998;39:928–934.
3. Pierpaoli C, Jezzard P, Basser PJ, Barnett A, Di Chiro G. Diffusion tensor MR imaging of the human brain. Radiology 1996;201:637–648.
4. Douek P, Turner R, Pekar J, Patronas N, Le Bihan D. MR color mapping of myelin fiber orientation. J Comput Assist Tomogr 1991;15:923–929.
5. Basser PJ, Pajevic S, Pierpaoli C, Duda J, Aldroubi A. In vivo fiber tractography using DT-MRI data. Magn Reson Med 2000;44:625–632.
6. Jones DK, Simmons A, Williams SC, Horsfield MA. Non-invasive assessment of axonal fiber connectivity in the human brain via diffusion tensor MRI. Magn Reson Med 1999;42:37–41.
7. Mori S, Crain BJ, Chacko VP, van Zijl PC. Three-dimensional tracking of axonal projections in the brain by magnetic resonance imaging. Ann Neurol 1999;45:265–269.
8. Poupon C, Mangin J, Clark CA, Frouin V, Regis J, Le Bihan D, Bloch I. Towards inference of human brain connectivity from MR diffusion tensor data. Med Image Anal 2001;5:1–15.
9. Riahi F, Zijdenbos A, Narayanan S, Arnold D, Francis G, Antel J, Evans AC. Improved correlation between scores on the expanded disability status scale and cerebral lesion load in relapsing-remitting multiple sclerosis. Results of the application of new imaging methods. Brain 1998;121:1305–1312.
10. Talairach J, Tournoux P. Co-planar stereotaxic atlas of the human brain. Stuttgart: Thieme Medical Publishers; 1988.
11. Conturo TE, Lori NF, Cull TS, Akbudak E, Snyder AZ, Shimony JS, McKinstry RC, Burton H, Raichle ME. Tracking neuronal fiber pathways in the living human brain. Proc Natl Acad Sci USA 1999;96: 10422–10427.
12. Bland M. An introduction to medical statistics. Oxford: Oxford University Press; 1993.
13. Stejskal E, Tanner J. Spin diffusion measurements: spin echoes in the presence of time-dependent field gradients. J Chem Phys 1965;42:288–292.
14. Morgan PS, Moody AR, Allder SJ, Bowtell RW. Correction of distortion in ADC maps using the reversed gradient method. In: Proceedings of the 8th Annual Meeting of ISMRM, Denver, 2000. p 800.
15. Skare S, Li T, Nordell B, Ingvar M. Noise considerations in the determination of diffusion tensor anisotropy. Magn Reson Imaging 2000;18:659–669.
16. Parker GJ, Schnabel JA, Symms MR, Werring DJ, Barker GJ. Nonlinear smoothing for reduction of systematic and random errors in diffusion tensor imaging. J Magn Reson Imaging 2000;11:702–710.
17. Westin CF, Maier SE, Khidhir B, Everett P, Jolesz FA, Kikinis R. Image processing for diffusion tensor magnetic resonance imaging. In: Proceedings of the 2nd Annual International Conference of MICCAI, Cambridge, 1999. p 441–452.
18. Boas M. Mathematical methods in the physical sciences. New York: John Wiley & Sons; 1983.
19. Press W, Teukolsky S, Vetterling W, Flannery B. Numerical recipes in C. Cambridge: Cambridge University Press; 1992.
20. Werring DJ, Clark CA, Barker GJ, Thompson AJ, Miller DH. Diffusion tensor imaging of lesions and normal-appearing white matter in multiple sclerosis. Neurology 1999;52:1626–1632.
21. Kernighan B, Ritchie D. The C programming language. New Jersey: Prentice Hall; 1988.
22. Virta A, Barnett A, Pierpaoli C. Visualizing and characterizing white matter fiber structure and architecture in the human pyramidal tract using diffusion tensor MRI. Magn Reson Imaging 1999;17:1121–1133.
23. Poupon C, Clark CA, Frouin V, Regis J, Bloch I, Le Bihan D, Mangin J. Regularization of diffusion-based direction maps for the tracking of brain white matter fascicles. Neuroimage 2000;12:184–195.
24. Martin KM, Papadakis NG, Huang CL, Hall LD, Carpenter TA. The reduction of the sorting bias in the eigenvalues of the diffusion tensor. Magn Reson Imaging 1999;17:893–901.
25. Filippi M, Cercignani M, Inglese M, Horsfield MA, Comi G. Diffusion tensor magnetic resonance imaging in multiple sclerosis. Neurology 2001;56:304–311.
26. Horsfield MA, Lai M, Webb SL, Barker GJ, Tofts PS, Turner R, Rudge P, Miller DH. Apparent diffusion coefficients in benign and secondary progressive multiple sclerosis by nuclear magnetic resonance. Magn Reson Med 1996;36:393–400.
27. Droogan AG, Clark CA, Werring DJ, Barker GJ, McDonald WI, Miller DH. Comparison of multiple sclerosis clinical subgroups using navigated spin echo diffusion-weighted imaging. Magn Reson Imaging 1999;17:653–661.
28. Filippi M, Iannucci G, Cercignani M, Assunta Rocca M, Pratesi A, Comi G. A quantitative study of water diffusion in multiple sclerosis lesions and normal-appearing white matter using echo-planar imaging. Arch Neurol 2000;57:1017–1021.
29. Christiansen P, Gideon P, Thomsen C, Stubgaard M, Henriksen O, Larsson HB. Increased water self-diffusion in chronic plaques and in apparently normal white matter in patients with multiple sclerosis. Acta Neurol Scand 1993;87:195–199.